Suppressing Lithium Migration in a Carbon Fiber Negative Electrode During Atom Probe Tomography Analysis

Suppressing Lithium Migration in a Carbon Fiber Negative Electrode During Atom Probe Tomography Analysis

Marcus Johansen, Mahander P Singh, Baptiste Gault, Fang Liu

Microscopy and Microanalysis, 2024, **30**, 1066–1073
https://doi.org/10.1093/mam/ozae058
Advance access publication 19 July 2024
Original Article

Microscopy AND Microanalysis

Suppressing Lithium Migration in a Carbon Fiber Negative Electrode During Atom Probe Tomography Analysis

Marcus Johansen[1], Mahander P. Singh[2], Baptiste Gault[2,3], and Fang Liu[1,*]

[1]*Department of Industrial and Materials Science, Chalmers University of Technology, SE-412 96 Gothenburg, Sweden*
[2]*Max-Planck-Institut für Eisenforschung GmbH, 40237 Düsseldorf, Germany*
[3]*Department of Materials, Imperial College London, Kensington, London SW7 2BP, UK*

***Corresponding author:** Fang Liu, E-mail: fang.liu@chalmers.se

Abstract

Carbon fibers can play dual roles, carrying mechanical load and hosting lithium (Li) simultaneously in multifunctional devices called structural batteries. It is essential to gain a detailed understanding on the interaction between Li and carbon fibers on the nanoscale. Atom probe tomography (APT) can potentially reveal individual Li and C atoms. However, lithiated carbon fibers experience massive Li migration once exposed to the electric field in the APT instrument. We show that a few nanometers of a chromium (Cr) coating on APT specimens can shield the electric field and suppress the massive Li migration. The related effects of the Cr coating, such as introduction of oxygen, enhanced mass resolving power of the mass spectrum, and increased portion of single hits, are also discussed.

Key words: conductive coating, delithiation, multifunctional composites, structural batteries

Graphical Abstract

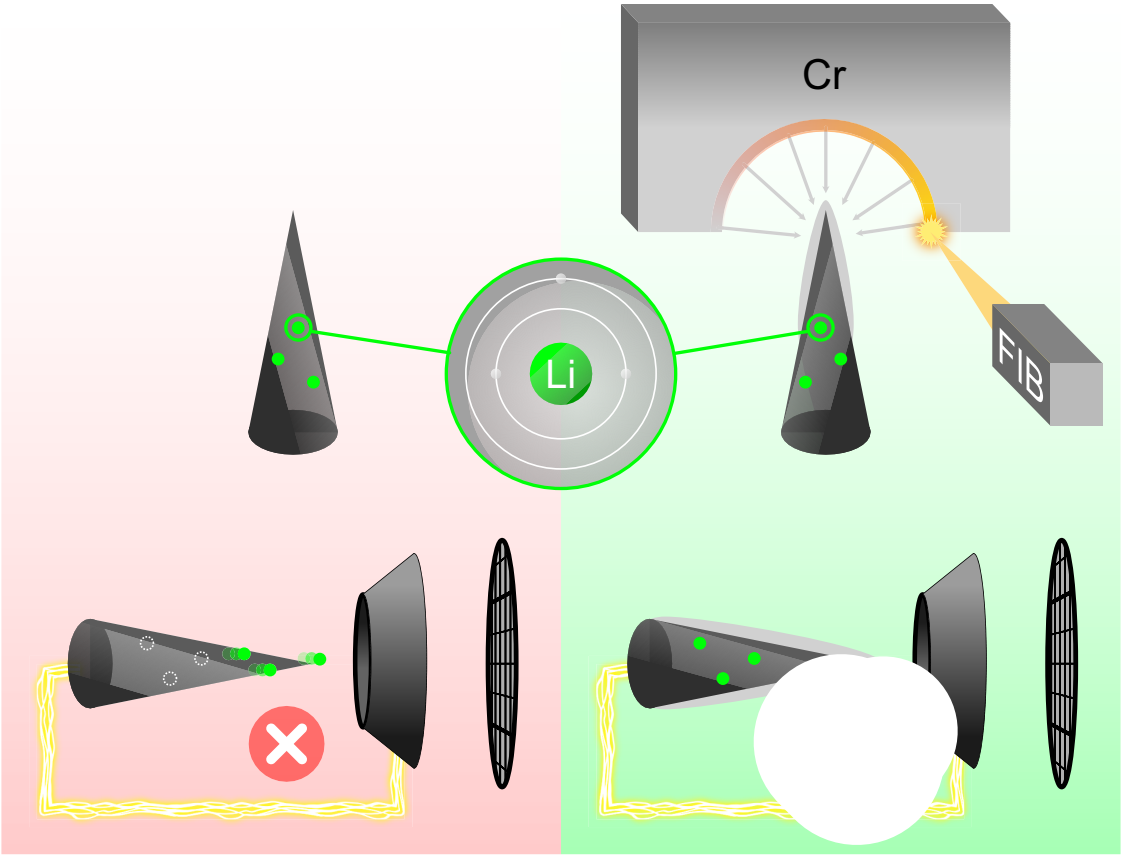

Received: November 27, 2023. **Revised:** April 15, 2024. **Accepted:** June 18, 2024

Introduction

Lithium (Li)-ion batteries power electric vehicles, enabling the transition to fossil-free transportation. However, today, almost all batteries are mono-functional, adding passive weight to the vehicle for the sole purpose of energy storage. Graphitic and hard carbons are the most widely used negative electrode materials in commercial Li-ion batteries, providing well-balanced properties and low cost (Asenbauer et al., 2020; Zhang et al., 2021). Carbon fibers with specific microstructures also show electrochemical properties close to those of commercial carbon materials (Hagberg et al., 2016). Given their superior mechanical properties, carbon fibers have been successfully used in multifunctional devices—structural batteries (Asp et al., 2019; Jin et al., 2022). These devices store energy as a Li-ion battery and simultaneously bear mechanical load as a carbon-fiber-reinforced composite. All the major components of the structural battery are multifunctional, including carbon fibers, which function as both negative electrode and structural reinforcements. By combining the energy storage and structural functions, the structural battery can, for instance, be installed as car panels, thus reducing the weight of electrical vehicles and further improving the overall environmental impact, according to recent life cycle analyses (Zackrisson et al., 2019; Hermansson et al., 2023).

The microstructure of different types of carbon fibers has been investigated and correlated to their electrochemical performance. Hagberg et al. (2016) have shown that intermediate-modulus carbon fibers perform remarkably better than high-modulus fibers as negative electrodes in structural batteries. The detailed microstructure of the two types of fibers has been studied using high-resolution transmission electron microscopy (Fredi et al., 2018), hard X-ray photoelectron spectroscopy, atom probe tomography (APT; Johansen et al., 2021), and X-ray scattering techniques (Xu et al., 2023). It has been revealed that intermediate-modulus carbon fibers contain both amorphous and crystalline domains, which are several nanometers in size. In addition to the predominant carbon (C) atoms, there are low concentrations of other elements (<5% collectively), nitrogen (N) and oxygen (O). Particularly, the chemical states of nitrogen play an important role in the energy capacity of carbon fibers (Johansen et al., 2021).

Although the interaction of Li with graphitic and hard carbons is well-understood, the interaction with carbon fibers remains largely unexplored. Recently, Auger electron spectroscopy (Johansen et al., 2023) and nuclear magnetic resonance (Fang et al., 2022) revealed the first details on how Li atoms interact with carbon fibers during electrochemical cycling. APT, with its unparalleled spatial resolution in three dimensions, has the potential to provide more microstructural and chemical details for a fundamental understanding. However, APT on carbon materials is inherently challenging (Nishikawa & Taniguchi, 2014; Lewis et al., 2015; Mukherjee et al., 2016; Jiang et al., 2017; Marceau et al., 2019; Ngo et al., 2020; Raghuwanshi et al., 2020). In our previous work, we used different specimen preparation geometries and optimized the acquisition parameters to enhance the mass resolving power of the mass spectra and thus deciphered the complex spectra of carbon fibers (Johansen & Liu, 2022). Based on the knowledge about APT on uncycled carbon fibers, in this study, we focus on how to use APT to reveal the microstructure of lithiated carbon fibers. We show that a conductive coating on the APT tip is essential to prevent electric field–induced massive migration of Li in the initial stage of the APT analysis. Furthermore, we reveal the interesting observation of low hydrogen (H) concentration in lithiated carbon fibers. We also elucidate the effects of a chromium (Cr) coating on the APT results.

Materials and Methods

Preparation of Lithiated Carbon Fibers

A thin carbon fiber tape T800SC-12k-50C (Oxeon AB), manufactured from T800 carbon fibers (Toray, Japan) in 12k (containing 12,000 fibers) yarns, was cut ~5 cm long and dried in a vacuum oven at 50°C overnight. Inside a glove box with dry argon atmosphere (<1 ppm H_2O, <1 ppm O_2), the fibers were assembled in a pouch cell, together with Li metal foil as the counter electrode, a Whatman glass microfiber paper as the separator, and a copper and a nickel strip as current collectors. Liquid electrolyte (1.0 M solution of Li hexafluorophosphate in diethyl carbonate and ethylene carbonate 50:50 wt%; Sigma-Aldrich) was added into the bag before the cell was vacuum-sealed. The cell was cycled with a Neware CT-4008-5V10mA-164 battery cycler using a current corresponding to 0.1C (10 h to fully charge an ideal cell with perfect graphite) for five cycles, and finally, at 0.05C for the last cycle until full charge (Xu et al., 2022). After cycling, the lithiated fibers were taken out from their cells, dried, adhered to scanning electron microscope (SEM) stubs with copper tape, and sealed again in a pouch bag before being taken out of the glove box and sent to the Max Planck Institute in Düsseldorf or transferred to other instruments at Chalmers University of Technology in Gothenburg.

Specimen Preparation for APT

The conventional *in situ* lift-out method using a combined focused ion beam (FIB) and SEM was used to prepare the APT specimens (Thompson et al., 2007). Two different workflows were followed to transfer the fibers into the FIB/SEM and then into APT at Chalmers University of Technology and the Max Planck Institute in Düsseldorf, respectively. For the first workflow, the fibers experienced quick exposure to air, estimated <10 min in total, until finally, the prepared APT specimen was kept under vacuum in APT. An FEI Versa 3D FIB/SEM was used. For the second workflow, the fibers were transferred under ultrahigh vacuum using a vacuum transfer system (Ferrovac). In order to shield the electrical field, some of the APT specimens were coated with redeposited Cr generated by FIB milling on a piece of pure Cr in the vicinity of the specimens (Douglas et al., 2023; Woods et al., 2023). A Thermo Fisher Scientific Helios5CX FIB/SEM was used in this case.

Atom Probe Tomography

Atom probe instruments such as an IMAGO LEAP 3000X HR, a CAMECA LEAP 5000 XR, and a CAMECA LEAP 5000 XS were used to analyze the lithiated carbon fibers. The LEAP 3000 has a green laser (wavelength 532 nm) and the LEAP 5000 instruments have an ultraviolet laser (wavelength 355 nm). The instruments were operated in the pulsed laser mode with a pulse energy of 1 nJ on LEAP 3000, and between 50 and 80 pJ on LEAP 5000, and a pulse frequency of 100 kHz. The specimens were held in the temperature range of 40–100 K. The acquired data were analyzed using the AP Suite software.

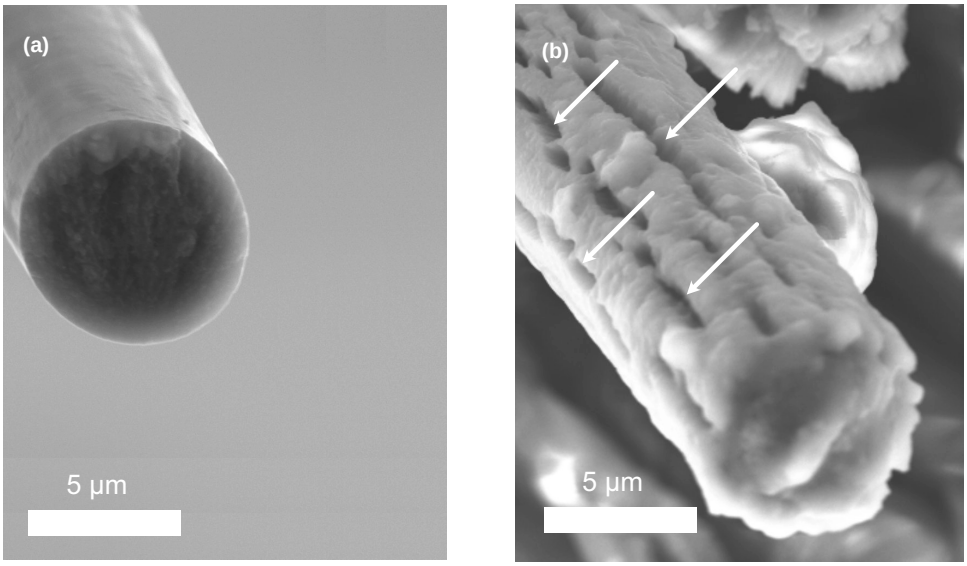

Fig. 1. A scanning electron microscope micrograph of (**a**) an uncycled carbon fiber, and (**b**) a lithiated carbon fiber after a 2-week exposure to air. Note the rather smooth surface of the uncycled fiber and the cracks (arrowed) formed through the surface oxide.

A rather big matrix is formed by carbon fiber specimens with various charge states, three types of APT instruments, and a range of APT operational parameters. Therefore, to facilitate the process of navigation for the readers, we summarize these factors into Supplementary Table S1 to provide an overview.

Results and Discussion

Transfer of Lithiated Carbon Fibers

Lithiated carbon fibers were transferred either under ultrahigh vacuum conditions or with short exposure to ambient air. These fibers are sensitive to air exposure; upon exposure, oxidation of Li occurs, leading to the formation of an oxide layer on the surface of the fibers (Fig. 1). There are two obvious drawbacks of air exposure: first, the chemical reactions change the original distribution of Li atoms; second, the formed oxide layer tends to suffer from sudden peel-off from the fiber substrate at the initial stage of the APT analyses and thus leads to premature specimen failures. The latter is due to the oxide's poor mechanical properties, which are demonstrated by the cracks formed through the surface oxide layer along a lithiated carbon fiber (Fig. 1). Note that this particular lithiated fiber had been exposed to air for 2 weeks. A much thinner oxide layer is expected to form on the APT tips because of the deliberately quick transfer and short air exposure time.

Success Rate of APT Analyses on Lithiated Carbon Fibers

Ambient air transfer of APT specimens has been shown to have somewhat positive effects, particularly for APT analyses of certain positive electrodes, in terms of improving the success rate of APT analyses and suppressing delithiation induced by the electric field in APT (Kim et al., 2022). However, air transfer does not increase the success rate of the APT analysis of lithiated carbon fibers. Uncycled carbon fibers are already challenging for APT, due to the extremely high evaporation field of C (>100 V/nm; Tsong, 1978), in combination with the nanopores in their microstructure (Johansen & Liu, 2022; Xu et al., 2023). Unfortunately, the Li ions inserted in the lithiated carbon fibers do not seem to fill the nanopores in a way that eases the APT data acquisition process. With the challenge posed by the surface oxides, we experienced even higher premature specimen failures than with uncycled fibers, obtaining only 4 good runs out of 20 prepared tips; for the uncycled fibers, we obtained 13 datasets, each containing >100,000 ions, out of a total of 40 attempts. In contrast, for APT specimens of lithiated fibers that were transferred in ultrahigh vacuum and coated with Cr, a remarkable increase was achieved in the success rate of acquisition, with two out of two specimens yielding useful results. There are two likely reasons for this: firstly, the ultrahigh vacuum transfer largely mitigates the formation of an Li oxide layer, thereby preventing sudden failure between the oxide and the lithiated carbon fiber; secondly, the Cr coating can promote a more homogenous field distribution, thus facilitating a smoother evaporation.

Premature specimen failure poses a big challenge in the analysis of lithiated carbon fibers using APT. Several factors can contribute to increased yield. Firstly, the use of a UV laser seems preferable over a green laser. This is also valid for a bare carbon fiber: only very short runs were obtained using a green laser, unless the specimen holding temperature was increased to 100 K. Many successful runs were obtained using a UV laser at 50 and 60 K. Another crucial factor is coating the APT specimen with a thin metal layer, as discussed above. On the other hand, the trends in factors such as laser energy are difficult to determine.

APT of Bare Lithiated Carbon Fibers

The so-called "*in situ* delithiation"—Li migration under the electric field in APT to the fiber surface and subsequent massive field evaporation of Li—occurs immediately as the APT specimen is exposed to the starting voltage of 0.5 kV (Supplementary Fig. S1). Only $^{6}Li^{+}$ and $^{7}Li^{+}$ peaks are observed in the mass spectrum, and almost all (98%) are detected as single hit ions (Supplementary Fig. S2). *In situ* delithiation was reported in the APT of $Li_2Mn_2O_4$, a positive electrode,

where delithiation was induced at a rather high temperature of 298 K and a high electric field >3 kV (Pfeiffer et al., 2017). Compared with the positive electrode, lithiated carbon fibers experience delithiation at a much lower temperature (<100 versus 298 K) and lower voltage (barely 0.5 versus >3 kV). After the completion of the delithiation process, in order to reach the set ion detection rate, the instrument voltage started to increase without any peaks being detected until above ~3 kV, when the field evaporation of both trapped Li and C starts. The initiation voltages for the C dominant part are comparable with that of our previous study on uncycled carbon fibers, which was ~3.5 kV (Johansen & Liu, 2022). This value also varies depending on the initial tip radius of the APT specimen. The reconstruction turns out to be a volume with a pure Li capping on a volume with predominant C and a small amount of Li (Fig. 2).

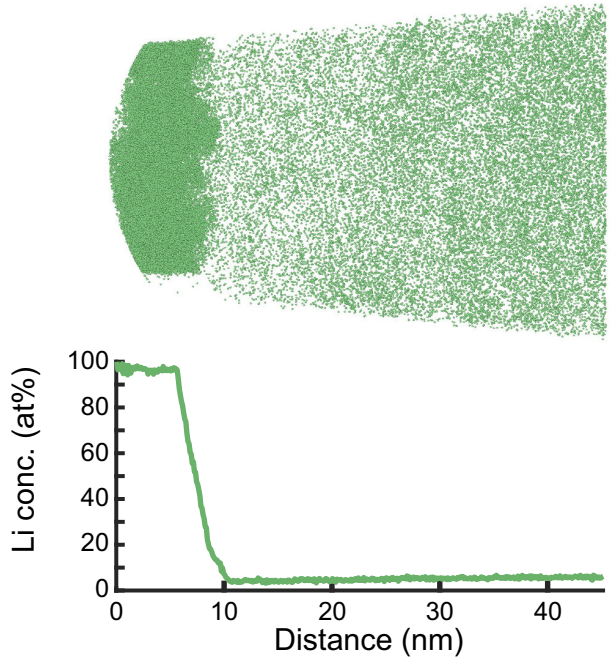

Fig. 2. An atom probe tomography reconstruction showing only lithium (Li) atoms for a lithiated carbon fiber experiencing massive evaporation of Li and the corresponding one-dimensional concentration profile of Li.

The massive delithiation in the initial stage of APT analysis is partly attributed to the weak bonds between C and Li. It is important to note that the bonds between the C and the Li are not covalent. For Li intercalation between graphene layers in graphite (a close-packed hexagonal structure), there is a weak bond between Li and the graphene rings—with Li sharing its outer electron with the graphene π bonds (Sole et al., 2014). In carbon fibers, even though the nature of insertion (not intercalation due to the lack of a layered structure) of Li into the amorphous domains and turbostratic graphene layers is still unclear, it is reasonable to assume that these C and Li bonds are also weak. Together with the weak bonds, the semiconductive nature of the intermediate-modulus carbon fiber, T800 (Toray, 2024), leads to delithiation, since the electric field in APT penetrates deep into semiconductors (Schwarz et al., 2024). Although not as profoundly as in insulators (Greiwe et al., 2014), the electric field applied to the APT specimen does penetrate into semiconductors. A lower electric voltage is expected at the apex of the APT specimen compared with at its base, similar to the voltage distribution shown by finite-element simulation by Adineh et al. (2017). Lithiated carbon fibers are electrochemically active. Thus, the field drives the migration of Li to the specimen apex, and Li then becomes field-evaporated (Belkacemi et al., 2023). Massive migration and accumulation of Li on lithiated carbon fibers and graphite was also reported, which was driven by a high electron current in Auger electron spectroscopy and SEM (Zhang et al., 2022; Johansen et al., 2023). There, it was also believed that a local field generated by the accumulated electrons was the underlying reason. Electric field penetration was also the reason for the initial delithiation of $Li_2Mn_2O_4$. However, in that case, the stronger interaction between Li and the oxide lattice required a higher temperature and voltage for Li migration to occur compared with lithiated carbon fibers.

Importantly, the delithiation process provides a unique opportunity to analyze the distribution of atoms in the original delithiated state without the interference of Li diffusion at ambient temperature and prolonged specimen preparation time. However, the initial massive delithiation in the APT hinders the analysis of the intact lithiated carbon fibers.

Carbon materials are known to be good candidates for H storage due to their adsorption capabilities (Mohan et al., 2019). Indeed, a significant amount of H was detected in uncycled fibers (~0.9%). However, in the lithiated fibers, the detected H-related peaks were small—a low H^+ peak and almost

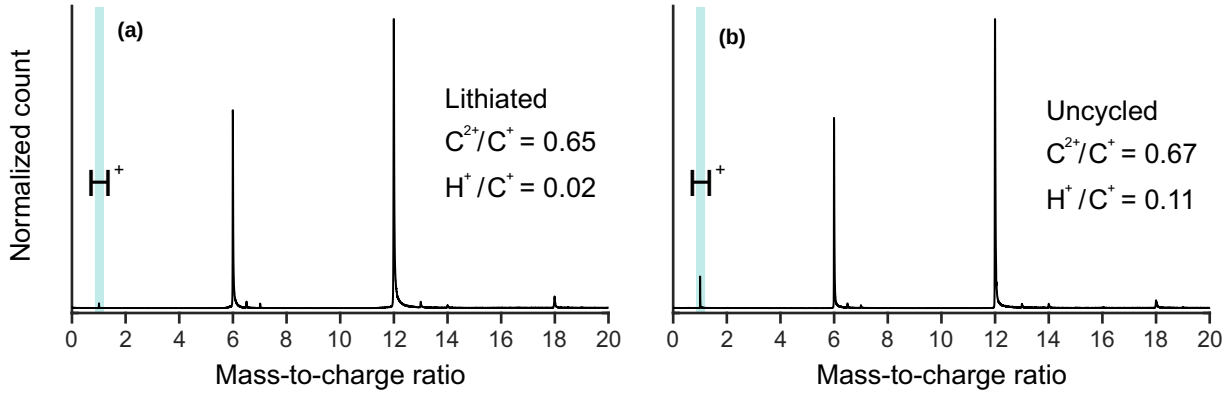

Fig. 3. Spectra between 0 and 20 Da obtained from (**a**) bare lithiated and (**b**) uncycled carbon (C) fibers, showing hydrogen (H), C, and lithium peaks. Note that the H peak is much higher in the uncycled fiber.

no H_2^+ and H_3^+ peaks (~0.1%; Fig. 3). Note that the ratio between C^{2+} and C^+ was nearly identical in these two runs, indicating a similar electric field for both. This ensures that any difference in H content is not caused by variations in the electric field. Yoo et al. (2022) elucidated the absence of H signals in alkali metals (Na and K) using experiment data and thermodynamic data generated from density functional theory. They concluded that H usually detected by APT experiments most likely originated from specimen preparation instead of gas residuals from the APT chamber. In this case, when many Li atoms interact with C in the lithiated carbon fibers, it is likely that fewer free locations are available for H. Consequently, the total H detected in a bare lithiated carbon fiber is much less than that in uncycled carbon fibers.

Effects of Cr Coating on APT of Lithiated Carbon Fibers

In order to analyze the original atomic distribution of lithiated carbon fibers, we protected the lithiated carbon fibers from air exposure using ultrahigh vacuum transfer from the glove box to the FIB/SEM and then to the APT; additionally, we deposited a conductive Cr layer covering the APT tips. As proposed by Kim et al. (2022), this conductive layer can form a Faraday's cage, preventing electric field penetration deeper below the layer, thereby suppressing the massive Li migration induced by the electric field. The results are significant and positive: without the coating, there is a cap of pure Li followed by a volume with a much lower Li concentration (~1.5%); with the coating, almost all Li ions are found distributed within the carbon fiber—the measured concentration (~9%) is rather close to the calculated theoretical value, 9.9% (see Supplementary Information). With the obtained APT datasets, we performed frequency distribution and nearest neighbor analyses. The results indicate that Li ions tend to agglomerate in lithiated carbon fibers, while the distribution tends to be random in delithiated fibers (Johansen et al., 2024).

Note that even though a pure Cr piece was used as the sputtering target, in the mass spectra from the Cr coating, there is a significant number of O-related ions (Fig. 4). This can be explained by Cr oxidizing at room temperature even at the extremely low O_2 partial pressure of $\sim 10^{-16}$ atm (Khanna, 2002), and the reaction kinetics occur at a fast pace. Thus, at least a part of the Cr in the coating is oxidized, which leads to an increased evaporation field compared with metallic Cr. In the case of analyzing the lithiated carbon fibers, since C has a very high evaporation field (~100 V/nm), it is advantageous to increase the evaporation field of the coating and yield a smoother transition from the coating to the carbon fiber during acquisition. However, in a material system where O is of interest, it may be beneficial to consider more noble metals such as nickel and silver as coating materials.

Additionally, a small amount of Cr was found deep in the carbon fiber, which is shown by the one-dimensional (1D) concentration profile retrieved from a thin cylinder (Fig. 4). In order to deposit the Cr layer to cover the APT tip, we used the 30 kV Ga ions from the FIB to bombard the Cr piece, and the sputtered material redeposited onto the tip. Secondary ions generated by the bombardment can gain up to 10% of the primary ion beam's energy (Fu et al., 2019). Thus, a small amount of Cr was implanted into the carbon fiber. Together, some O ions are also expected to be implanted, which is further discussed below. The coating parameters can be further optimized for carbon materials to minimize Cr and O implantation. A much lower primary ion beam energy may decrease implantation from the coating material. Additionally, more noble metals, with lower O affinity, can be used as the target material to reduce the O content.

The mass spectra obtained from the bare and Cr-coated lithiated carbon fibers were compared (Fig. 5). Both spectra were obtained by using the LEAP 5000 XR and extracted from volumes with the same number of ions, $\sim 2 \times 10^6$. Note that the significant H-related peaks in the spectrum of Cr-coated fibers were mostly linked to the Cr coating. Again, despite the prevalent Cr- and O-related peaks

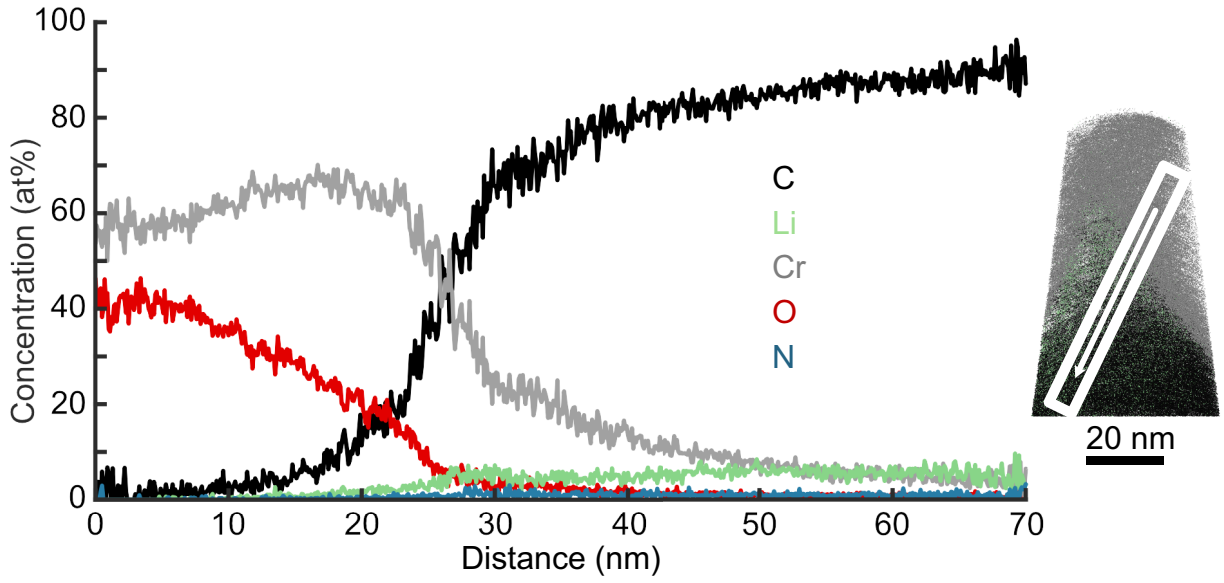

Fig. 4. A one-dimensional concentration profile for carbon, lithium, chromium (Cr), oxygen, and nitrogen over the interface between the Cr coating and the lithiated carbon fiber.

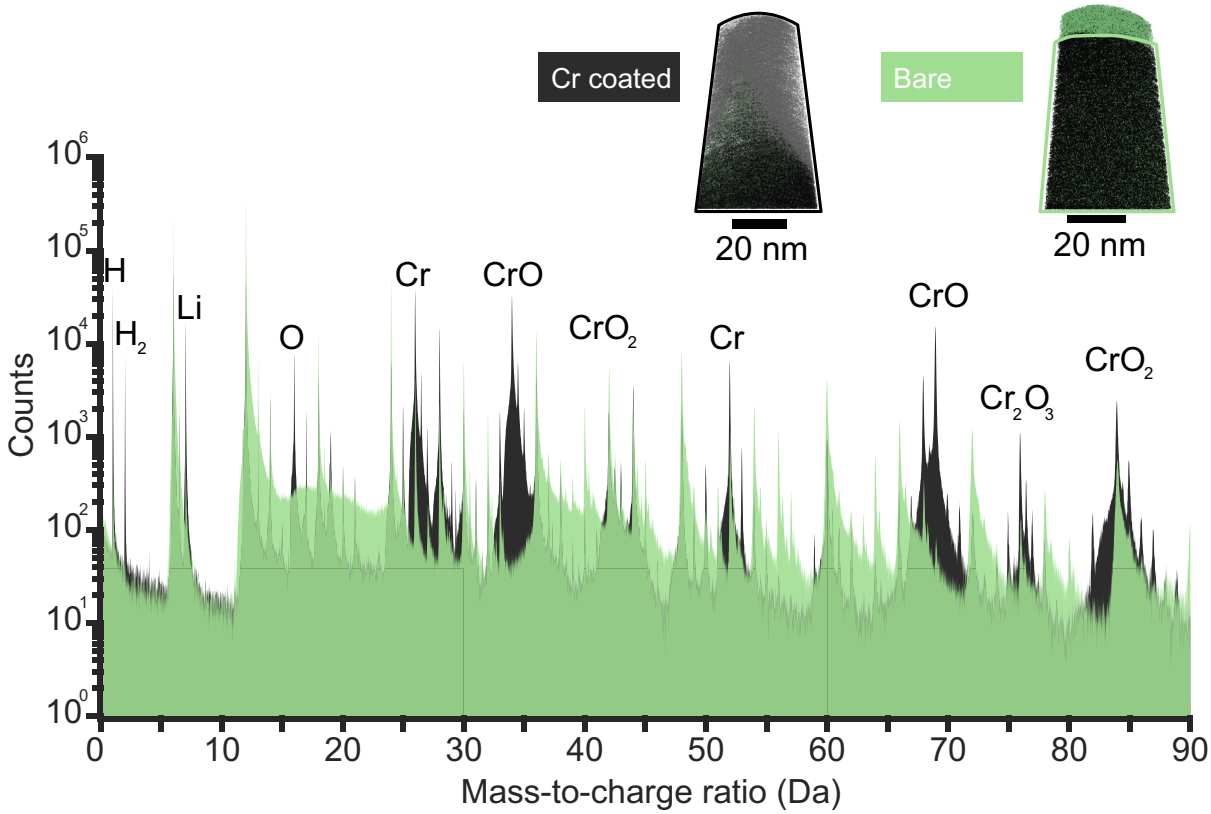

Fig. 5. A comparison of spectra from bare and chromium (Cr)-coated lithiated carbon fibers. Some of the peaks introduced by the Cr coating are marked. Note that the lithium (Li) peak at 7 Da is pronounced for the Cr-coated fiber, as the coating prevents the initial massive migration of Li. Also, the Cr coating contains a significant amount of oxygen.

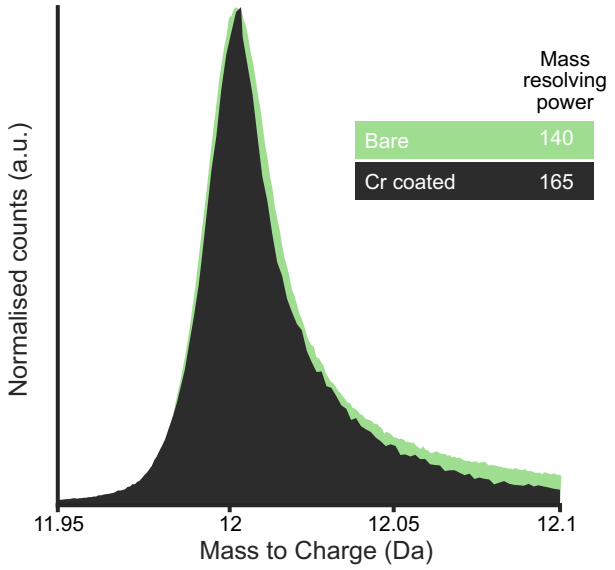

Fig. 6. The mass resolving power of the peak at 12 Da from bare and chromium-coated lithiated carbon fibers.

(predominantly from the coating), a large amount of Li was detected in the Cr-coated fiber, while only a small amount of Li were left in the bare lithiated carbon fiber due to the massive initial delithiation. Obviously, the spectrum obtained from the bare lithiated carbon fiber exhibited a few times higher background (note that the *y*-axis was in a logarithmic scale). As an intermediate-modulus carbon fiber, T800 has a relatively poor thermal conductivity: 35 W/(m K) along the axial direction, and 5 W/(m K) across the transverse direction (Kurita et al., 2014; Toray, 2020). With the geometry used for specimen preparation, the transverse direction of the carbon fiber is placed along the APT specimen axis, leading to a poor thermal conductivity away from the APT tip. Hence, with a much higher thermal conductivity (94 W/(m K)), Cr coating can dissipate the heat from laser pulses faster (Moore et al., 1977). Additionally, Cr can more significantly reflect the incident laser beam compared with bare carbon fibers. Graphite has been reported to interact strongly with laser and convert the absorbed energies into thermal energy (Freitag et al., 2014). Therefore, smaller thermal tails are found in the spectrum of Cr-coated carbon fiber. The mass resolution power calculated at the full-width-half-maximum for the C peak at 12 Da is thus higher for the Cr-coated carbon fibers than for the bare lithiated carbon fibers, 580 versus 485 (Fig. 6).

Table 1. The percentage of single versus multiple hits of a bare lithiated carbon fiber, a Cr-coated lithiated carbon fiber, and the Cr coating itself.

	Single (%)	Multiple (%)
Bare lithiated carbon fiber	28	72
Cr-coated lithiated carbon fiber	44	56
Cr coating	80	20

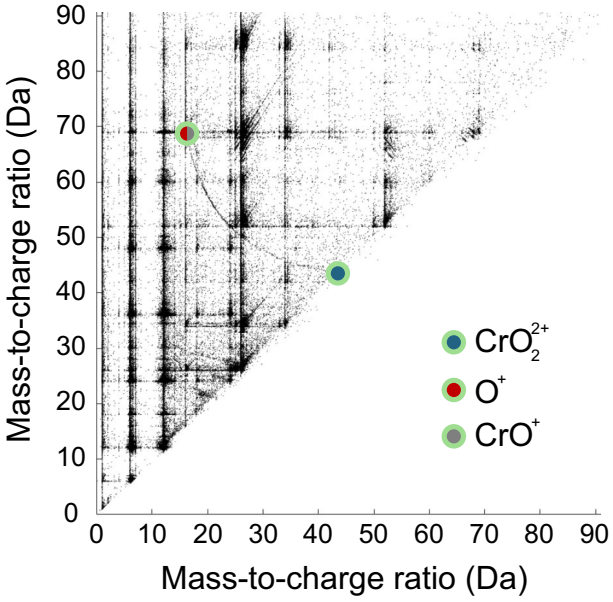

Fig. 7. A correlation histogram of a chromium (Cr)-coated lithiated carbon fiber. The marked coordinates correspond to CrO_2^{2+}, O^+, and CrO^+.

Furthermore, the Cr coating decreases the proportion of multiple hits (Table 1). For the bare lithiated carbon fiber, the percentage of multiple hits is as high as 72%, but with the coating, it decreases to 56%. The reason for this is likely linked to the decreased electric field with the conductive coating. For the Cr coating, the percentage of multiple hits is 20%, which confirms the partially oxidized nature of the coating, since pure metal usually exhibits multiple hits <10%.

Looking closer at the multiple hits in correlation histograms, it was found that none of the C-containing molecular ions experience dissociation into smaller ions during the flight to the detector. However, dissociation tracks are clearly seen for molecular ions related to the Cr coating (Fig. 7). Curved dissociation tracks from coordinates (42 Da, 42 Da) to (16 Da, 68 Da) indicate a dissociation of CrO_2^{2+} into CrO^+ and O^+. This reaffirms that the Cr coating contains O and may lead to an implantation of O into the carbonaceous material. Indeed, the content of O in the Cr-coated lithiated fiber is higher than that in the bare fiber (1.4 ± 0.3 versus 0.8 ± 0.3 at%).

Conclusions

APT on lithiated carbon fibers is rendered challenging due to the quick reaction with ambient air and fast Li migration in the electric field. *In situ* delithiation provides some insights into the original Li distribution in the delithiated state. However, to map the original Li distribution in lithiated carbon fibers, a conductive coating is essential, which prevents field penetration into the semiconductive carbon fiber and consequently suppresses the massive Li migration at the very initial stage of APT analysis. Less H was found in the lithiated carbon fibers during APT analyses. Additionally, the Cr coating improves the thermal conductivity of the APT specimen, thus increasing the mass resolution of the obtained spectra; it also decreases the voltage needed for field evaporation of the carbon fiber, thus increasing the portion of single hits and lowering the background level. However, the FIB-milling-induced redeposition process for Cr coating may introduce Cr and O implantation into the carbon fiber.

Availability of Data and Materials

The authors have declared that no datasets apply for this piece.

Supplementary Material

To view supplementary material for this article, please visit https://doi.org/10.1093/mam/ozae058.

Acknowledgments

The authors thank Dr Johanna Xu for providing the lithiated and delithiated fibers. They also thank Uwe Tezins, Christian Broß, and Andreas Sturm for their support in facilitating access to the FIB and APT facilities at MPIE.

Financial Support

This work was financially supported by the Swedish Energy Agency (Project no. 46598-1). F.L. thanks the strategic innovation program LIGHTer (funding provided by Vinnova, the Swedish Energy Agency and Formas). M.S. is grateful for receiving funding from the MPIE scholarship.

Conflict of Interest

The authors declare that they have no competing interest.

References

Adineh VR, Marceau RKW, Chen Y, Si KJ, Velkov T, Cheng W, Li J & Fu J (2017). Pulsed-voltage atom probe tomography of low conductivity and insulator materials by application of ultrathin metallic coating on nanoscale specimen geometry. *Ultramicroscopy* **181**, 150–159. https://doi.org/10.1016/j.ultramic.2017.05.002

Asenbauer J, Eisenmann T, Kuenzel M, Kazzazi A, Chen Z & Bresser D (2020). The success story of graphite as a lithium-ion anode material-fundamentals, remaining challenges, and recent developments including silicon (oxide) composites. *Sustain Energy Fuels* **4**, 5387–5416. https://doi.org/10.1039/D0SE00175A

Asp LE, Johansson M, Lindbergh G, Xu J & Zenkert D (2019). Structural battery composites: A review. *Funct Compos Struct* **1**, 042001. https://doi.org/10.1088/2631-6331/ab5571

Belkacemi LT, Gault B, Esin VA & Epp J (2023). Ga-induced delithiation of grain boundaries in a Li containing Al-based alloy. *Mater Charact* **199**, 112812. https://doi.org/10.1016/j.matchar.2023.112812

Douglas JO, Conroy M, Giuliani F & Gault B (2023). In situ sputtering from the micromanipulator to enable cryogenic preparation of specimens for atom probe tomography by focused-ion beam. *Microsc Microanal* **29**, 1009–1017. https://doi.org/10.1093/micmic/ozad020

Fang Y, Peuvot K, Gratrex A, Morozov EV, Hagberg J, Lindbergh G & Furó I (2022). Lithium insertion in hard carbon as observed by 7Li NMR and XRD. The local and mesoscopic order and their relevance for lithium storage and diffusion. *J Mater Chem A* **10**, 10069–10082. https://doi.org/10.1039/D2TA00078D

Fredi G, Jeschke S, Boulaoued A, Wallenstein J, Rashidi M, Liu F, Harnden R, Zenkert D, Hagberg J, Lindbergh G, Johansson P, Stievano L & Asp LE (2018). Graphitic microstructure and performance of carbon fibre Li-ion structural battery electrodes. *Multifunct Mater* **1**, 015003. https://doi.org/10.1088/2399-7532/aab707

Freitag C, Weber R & Graf T (2014). Polarization dependence of laser interaction with carbon fibers and CFRP. *Opt Express* **22**, 1474. https://doi.org/10.1364/OE.22.001474

Fu T, Della-Negra S, Touboul D & Brunelle A (2019). Internal energy distribution of secondary ions under argon and bismuth cluster bombardments: "soft" versus "hard" desorption–ionization process. *J Am Soc Mass Spectrom* **30**, 321–328. https://doi.org/10.1007/s13361-018-2090-z

Greiwe G-H, Balogh Z & Schmitz G (2014). Atom probe tomography of lithium-doped network glasses. *Ultramicroscopy* **141**, 51–55. https://doi.org/10.1016/j.ultramic.2014.03.007

Hagberg J, Leijonmarck S & Lindbergh G (2016). High precision coulometry of commercial PAN-based carbon fibers as electrodes in structural batteries. *J Electrochem Soc* **163**, A1790–A1797. https://doi.org/10.1149/2.0041609jes

Hermansson F, Edgren F, Xu J, Asp LE, Janssen M & Svanström M (2023). Climate impact and energy use of structural battery composites in electrical vehicles—A comparative prospective life cycle assessment. *Int J Life Cycle Ass* **28**, 1366–1381. https://doi.org/10.1007/s11367-023-02202-9

Jiang K, Siahrostami S, Akey AJ, Li Y, Lu Z, Lattimer J, Hu Y, Stokes C, Gangishetty M, Chen G, Zhou Y, Hill W, Cai WB, Bell D, Chan K, Nørskov JK, Cui Y & Wang H (2017). Transition-metal single atoms in a graphene shell as active centers for highly efficient artificial photosynthesis. *Chem* **3**, 950–960. https://doi.org/10.1016/j.chempr.2017.09.014

Jin T, Singer G, Liang K & Yang Y (2022). Structural batteries: Advances, challenges and perspectives. *Mater Today* **62**, 151–167. https://doi.org/10.1016/j.mattod.2022.12.001

Johansen M & Liu F (2022). Best practices for analysis of carbon fibers by atom probe tomography. *Microsc Microanal* **28**, 1092–1101. https://doi.org/10.1017/S1431927621012812

Johansen M, Schlueter C, Tam PL, Asp LE & Liu F (2021). Mapping nitrogen heteroatoms in carbon fibres using atom probe tomography and photoelectron spectroscopy. *Carbon N Y* **179**, 20–27. https://doi.org/10.1016/j.carbon.2021.03.061

Johansen M, Singh M, Xu J, Asp LE, Gault B & Liu F (2024). Unravelling lithium distribution in carbon fibre electrodes for structural batteries with atom probe tomography. *Carbon N Y* **225**, 119091. https://doi.org/10.1016/j.carbon.2024.119091

Johansen M, Xu J, Tam PL, Asp LE & Liu F (2023). Lithiated carbon fibres for structural batteries characterised with Auger electron spectroscopy. *Appl Surf Sci* **627**, 157323. https://doi.org/10.1016/j.apsusc.2023.157323

Khanna AS (2002). Introduction high temp oxidation of metals. In *Introduction High Temp Oxidation of Metals*, pp. 3. ASM International.

Kim SH, Antonov S, Zhou X, Stephenson LT, Jung C, El-Zoka AA, Schreiber DK, Conroy M & Gault B (2022). Atom probe analysis of electrode materials for Li-ion batteries: Challenges and ways forward. *J Mater Chem A* **10**, 4926–4935. https://doi.org/10.1039/D1TA10050E

Kurita H, Feuillet E, Guillemet T, Heintz JM, Kawasaki A & Silvain JF (2014). Simple fabrication and characterization of discontinuous carbon fiber reinforced aluminum matrix composite for lightweight heat sink applications. *Acta Metall Sin* **27**, 714–722. https://doi.org/10.1007/s40195-014-0106-7

Lewis JB, Isheim D, Floss C & Seidman DN (2015). 12C/13C-ratio determination in nanodiamonds by atom-probe tomography. *Ultramicroscopy* **159**, 248–254. https://doi.org/10.1016/j.ultramic.2015.05.021

Marceau RKW, Taylor AS, Sato T, Ringer SP, Fox BL, Stanford N & Henderson LC (2019). Local electrode atom probe tomography of carbon fibre. *Microsc Microanal* **25**, 2496–2497. https://doi.org/10.1017/S1431927619013217

Mohan M, Sharma VK, Kumar EA & Gayathri V (2019). Hydrogen storage in carbon materials—A review. *Energy Storage* **1**, e35. https://doi.org/10.1002/est2.35

Moore JP, Williams RK & Graves RS (1977). Thermal conductivity, electrical resistivity, and Seebeck coefficient of high-purity chromium from 280 to 1000 K. *J Appl Phys* **48**, 610–617. https://doi.org/10.1063/1.323697

Mukherjee S, Watanabe H, Isheim D, Seidman DN & Moutanabbir O (2016). Laser-assisted field evaporation and three-dimensional atom-by-atom mapping of diamond isotopic homojunctions. *Nano Lett* **16**, 1335–1344. https://doi.org/10.1021/acs.nanolett.5b04728

Ngo C, Fitzgerald MA, Dzara MJ, Strand MB, Diercks DR & Pylypenko S (2020). 3D atomic understanding of functionalized carbon nanostructures for energy applications. *ACS Appl Nano Mater* **3**, 1600–1611. https://doi.org/10.1021/acsanm.9b02360

Nishikawa O & Taniguchi M (2014). Atomic level analysis of carbon fibers by the scanning atom probe. *Surf Interface Anal* **46**, 1231–1235. https://doi.org/10.1002/sia.5695

Pfeiffer B, Maier J, Arlt J & Nowak C (2017). In situ atom probe deintercalation of lithium-manganese-oxide. *Microsc Microanal* **23**, 314–320. https://doi.org/10.1017/S1431927616012691

Raghuwanshi M, Cojocaru-Mirédin O & Wuttig M (2020). Investigating bond rupture in resonantly bonded solids by field evaporation of carbon nanotubes. *Nano Lett* **20**, 116–121. https://doi.org/10.1021/acs.nanolett.9b03435

Schwarz TM, Woods E, Singh MP, Chen X, Jung C, Aota LS, Jang K, Krämer M, Kim S-H, McCarroll I & Gault B (2024). In situ metallic coating of atom probe specimen for enhanced yield, performance, and increased field-of-view. *Microsc Microanal*, ozae006. https://doi.org/10.1093/mam/ozae006

Sole C, Drewett NE & Hardwick LJ (2014). Insitu Raman study of lithium-ion intercalation into microcrystalline graphite. *Faraday Discuss* **172**, 223–237. https://doi.org/10.1039/C4FD00079J

Thompson K, Lawrence D, Larson DJ, Olson JD, Kelly TF & Gorman B (2007). In situ site-specific specimen preparation for atom probe tomography. *Ultramicroscopy* **107**, 131–139. https://doi.org/10.1016/j.ultramic.2006.06.008

Toray (2020). Types of carbon fiber. Available at https://www.toraycma.com/page.php? id=661 (accessed November 30, 2020).

Toray (2024). https://www.toraycma.com/wp-content/uploads/T800S-Technical-Data-Sheet-1.pdf (accessed May 2024).

Tsong TT (1978). Field ion image formation. *Surf Sci* **70**, 211–233. https://doi.org/10.1016/0039-6028(78)90410-7

Woods EV, Singh MP, Kim S, Schwarz TM, Douglas JO, El-Zoka A, Giulani F & Gault B (2023). A versatile and reproducible cryo-sample preparation methodology for atom probe studies. *Microsc Microanal* **29**(6), 1992–2003. https://doi.org/10.1093/micmic/ozad120

Xu J, Creighton C, Johansen M, Liu F, Duan S, Carlstedt D, Mota-Santiago P, Lynch P & Asp LE (2023). Effect of tension during stabilization on carbon fiber multifunctionality for structural battery composites. *Carbon N Y* **209**, 117982. https://doi.org/10.1016/j.carbon.2023.03.057

Xu J, Geng Z, Johansen M, Carlstedt D, Duan S, Thiringer T, Liu F & Asp LE (2022). A multicell structural battery composite laminate. *EcoMat* **4**, e12180. https://doi.org/10.1002/eom2.12180

Yoo SH, Kim SH, Woods E, Gault B, Todorova M & Neugebauer J (2022). Origins of the hydrogen signal in atom probe tomography: Case studies of alkali and noble metals. *New J Phys* **24**, 013008. https://doi.org/10.1088/1367-2630/ac40cd

Zackrisson M, Jönsson C, Johannisson W, Fransson K, Posner S, Zenkert D & Lindbergh G (2019). Prospective life cycle assessment of a structural battery. *Sustainability* **11**, 5679. https://doi.org/10.3390/su11205679

Zhang H, Yang Y, Ren D, Wang L & He X (2021). Graphite as anode materials: Fundamental mechanism, recent progress and advances. *Energy Storage Mater* **36**, 147–170. https://doi.org/10.1016/j.ensm.2020.12.027

Zhang Y, Zhai W, Hu X, Jiang Y, Chen S, Zhang Y, Liu W & Yu Y (2022). Application of Auger electron spectroscopy in lithium-ion conducting oxide solid electrolytes. *Nano Res* **3**, 1–10.